Influence of aluminum addition on the laser powder bed fusion of copper-aluminum mixtures

Nada Kraiem, Loic Constantin, Aofei Mao, Fei Wang, Bai Cui, Jean-François Silvain, Yong Feng Lu

Study of the influence of Aluminum addition on the Laser Powder Bed Fusion of Cu-Al mixtures

Nada Kraiem,[1,2,‡,] Loic Constantin,[1,2‡,] Aofei Mao,[1,] Fei Wang,[3,] Bai Cui,[3,] Jean-François Silvain[1,2,] and, Yong Feng Lu,[1,]**

[1] Department of Electrical and Computer Engineering, University of Nebraska, Lincoln, NE, 68588-0511, USA.

[2] CNRS, Univ. Bordeaux, Bordeaux INP, ICMCB, UMR 5026, F-33608 Pessac, France.

[3] Department of Mechanical and Materials Engineering, University of Nebraska-Lincoln, Lincoln, NE 68588-0526.

Abstract:

The high optical reflectivity of copper (Cu) in the near infrared (NIR) domain and its elevated heat dissipation make Cu a challenging metal for laser powder bed fusion (LPBF), even with high energy densities (EDs). In this study, we demonstrated that adding aluminum (Al) powder by as little as 0.75, 1.5, and 3 wt.% substantially enhances Cu processability, leading to denser (up to 98 %) and smoother (Ra = 3.3 μm) Cu-Al parts as compared to 95% and 18 μm, respectively, for the parts printed using pure Cu. In addition, this method reduces the ED required by a factor of two for the additive manufacturing of the Cu-based parts while maintaining a significant heat dissipation. These improvements are achieved due to the coexistence of solid Cu particles with liquid Al at the vicinity of the molten pool, accomodating the predensification of the powder mixture. The development of the semi-liquid 3D printing

approach opens up a new path to easily print materials difficult to be printed for broadening their applications.

Keywords: Additive manufacturing, copper, aluminum, selective laser melting

Introduction

Selective laser melting (SLM) or laser powder bed fusion (LPBF), is an additive manufacturing process that enables the possibility of creating complex three-dimensional (3D) structures, where post-processing steps are reduced [1,2]. The diversity of the materials being processed has enabled the additive manufacturing (AM) techniques to produce functional components with ideal surface finishes and physical properties comparable to those of bulk materials [3]. In thermal management applications for example, Cu-based materials are ideal candidates due to their exceptional thermal properties. However, due to its high thermal conductivity (TC) and low laser absorption in the NIR region (less than 10%), high energy densities (EDs) must be applied on Cu powder beds to achieve a proper melting/solidification process [4,5].

Over the past decades, extensive research has been devoted to efficiently print pure Cu. Jadhav *et al.* [6] showed the printing of high-density Cu parts (99%) using a high laser power of 800 W. Nevertheless, the high reflection of Cu powders induces laser back reflection, leading to the damage of the laser source.

More recently, Constantin *et al.* [7] have used a lower energy density with a moderate laser power of 400 W. Dense (95%) and smooth Cu parts were printed. However, the processing window is very narrow, where an insufficient or excessive energy density has a great impact on the dynamics of the molten pool, and has significanly reduced the density down to 70%. Even

though dense parts were obtained, the LPBF of dense Cu parts is still challenging due to the thermal issues and reflective behaviors of Cu powders.

On the other hand, numerous studies have been carried out for the production of dense Cu alloys, such as Cu-Sn, Cu-Zn and Cu-Cr [8], where the laser absorption was improved up to 70% during the printing. However, it was noticed that the TC of the materials was severely degraded.

In this research, small amount of a lightweight metal was added to Cu powders. Having a relatively low melting point compared to Cu, it was demonstrated that Al forms a liquid metal that coexists with the solid Cu particles at the vicinity of the molten pool. Consequently, the heated Al softens the Cu particles and facilitates to create connections among them. Here, the liquid phase sintering (LPS) approach was applied during SLM to assist the densification of the Cu-Al mixtures [9,10]. It was found that high energy densities were no longer needed, and that high-density parts were successfully achieved.

Experimental procedure

Laser powder bed fusion of Cu-Al mixtures. Irregular Al (US Nano, 30 um, 99.7%) and spherical Cu powders (US Nano, 45 um, 99.5%) were added to form three mixtures of Cu with 0.75, 1.5, and 3.0 wt.% of Al, respectively **(Figure 1S)**.

The LPBF of Cu-Al parts was carried out using a SLM 125 HL system (SLM Solutions Inc) equipped with a continuous wave (CW) fiber laser (IPG photonics, YLM, Yb: YAG, λ = 1070 nm). The laser has a maximum power of 400 W and is focused on the powder bed with a spot diameter of 70 µm. The SLM was operated under a constant argon (Ar) flow to keep the oxygen level low at 0.1%. A pressure of 18 mbar was maintained inside of the printing chamber. Constantin et *al.* have shown that dense and crack-free pure Cu parts were additively

manufactured at a laser power of 400 W, a scan speed of 400 mm/s and a hatch distance of 0.12 mm [7]. Therefore, the choice of the processing parameters for the Cu-Al mixtures was based on their work. A laser power of 400 W and a layer thickness of 30 µm were used in the 3D printing experiments. The laser scan speed was varied from 300 to 800 mm/s at an increment of 100 mm/s. The hatch distance was varied from 0.06 to 0.16 mm at an increment of 0.02 mm.

The ED (J/mm^3) was calculated with the following equation:

$$ED = \frac{P}{LT \times h \times s}, \quad (1)$$

where P is the laser power (W), LT is the layer thickness (mm), h is the hatch distance (mm), and s is the scan speed (mm/s). The structures were initially drawn using Solidwork® and transferred in Magics® software to prepare the build jobs and fix the printing parameters. The parts were printed on a stainless-steel building plate (125 × 125 × 25 mm^3).

Characterization of the Cu-Al parts. The density of the samples was measured using the Archimedes method (Mettler Toledo AT201). The microstructures of the top surfaces of the samples as well as the Cu-Al powders were analyzed using a scanning electron microscope (SEM, FEI Quanta 200 Environmental SEM). The average surface roughness was characterized with an optical surface profiler (Zygo NewView 8000). Energy dispersive spectroscopy (EDS) was performed for chemical composition analysis using an X-Ray detector in the SEM (FEI Nova NanoSEM 450). The crystallinity of both the powders and the parts printed were analyzed by X-ray diffraction (XRD, PANalitycal X`pert PRO MPD diffractometer with a Cu Kα radiation source, λ = 0.154 nm). A high-resolution transmission electron microscopy (HR-TEM, FEI Tecnai Osiris) was used to analyze the microstructures of the parts printed.

The thermal dissipation performances of the printed gyroid structures made of pure Cu and Cu-Al at 3 wt.% Al, respectively, were also evaluated. An IR camera (FLIR E85 24°) was used during the recreation of a microelectronics thermal management situation. The parts printed were attached to an electronic chip using a thermal tape (3M™ 8815 Thermal Tape). The entire system was heated to 200 ºC. An airflow was assured by a fan placed 10 cm away from the parts.

Results and discussion

Several approaches have been implemented to achieving pore-free Cu parts by applying a moderate laser power on the powder bed. The in-situ alloying strategy in SLM was shown to be a potential method that enables a proper 3D printing of highly reflective powders such as Cu and Al [11]. However, the production of Cu-Al mixtures with a Cu-rich powder was not reported in the literature, which motivated our research to study the densification mechanism and processability of this mixture.

The optimization of the processing parameters and the evaluation of the printing quality were mainly based on the part density and surface finish. The relative density with respect to the hatch distance and scan speed are plotted in **Figure 1**. As can be seen on **Figure 1a**, the area showing high density (> 95%) of pure Cu parts was acquired within a very narrow processing window. Adding 0.75 wt.% Al in pure Cu has increased the density of the samples at scan speeds ranged between 600 and 700 mm/s, leading to a lower color contrast in **Figure 1b.** Note that the samples with 0.75 wt.% Al printed at a low scan speed of 300 mm/s peeled off from the building plate, and were not included in the characterization. When a high ED is applied, the liquid Cu was overheated, which generates a large thermal gradient in the solidified metal. The interlayer delamination occurred, causing the debonding of the parts from the plate [12].

For the 1.5 wt.% Al composition, **Figure 1c** shows a large area where the density is above 95%, extending from 350 to 800 mm/s. However, increasing the Al content to 3 wt.% reduced the sample densities as compared with the case of 1.5 wt.% Al, indicated by the shrinkage of the zone corresponding to the density above 95%. The densification upon the melting/solidification process of the powder depends on the laser-matter interactions [13]. Thus, the metallurgical properties of the powder and the processing parameters, such as the laser power, the scan speed, and the hatch distance, control the dynamics of the molten pool, and hence determines the printing quality of the final parts [14].

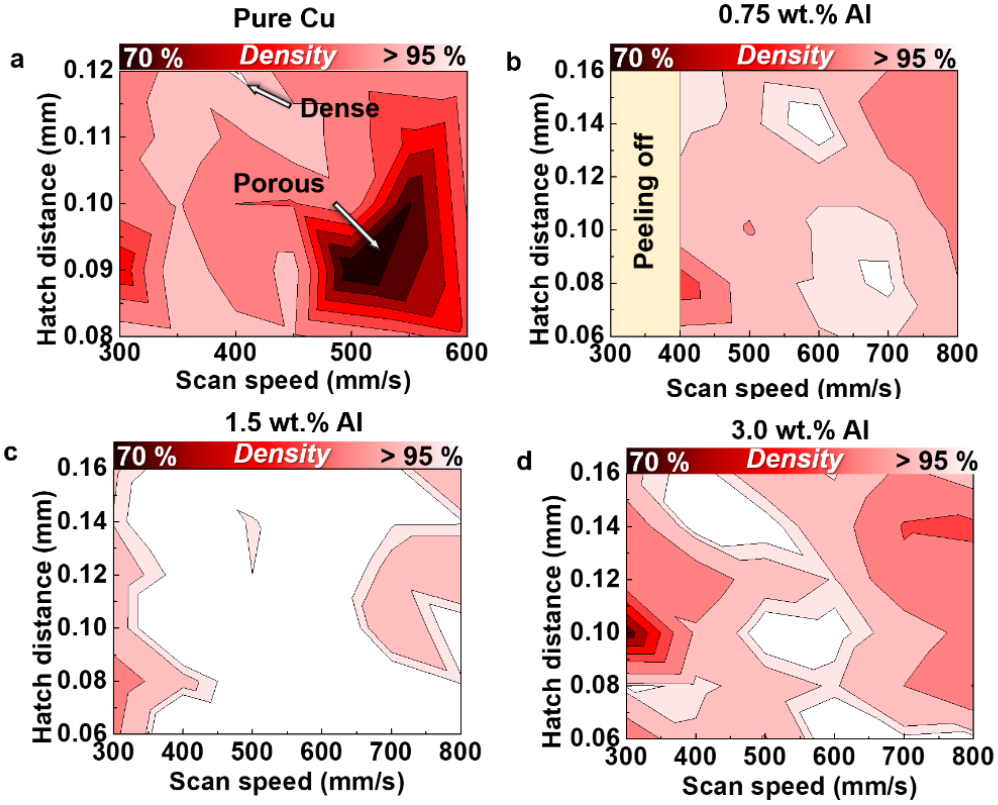

Figure 1. 2D maps of the relative density with respect to the hatch distance and the scan speed, **a** Pure Cu [7], and Cu with **b** 0.75, **c** 1.5, and **d** 3 wt.% Al.

As can be seen, the addition of a small amount of Al has enabled the printing of dense Cu-Al parts (98%) with lower EDs than those used to print pure Cu. The Al added has improved the densification of the powders and enhanced the fusion among the Cu particles.

To further understand the previous results of the density for each Cu-Al composition, the surface morphology of the samples was studied. **Figure 2** illustrates the variation of the density and the surface quality of the as-printed Cu-Al parts with respect to their Al content. As can be observed, the influence of the added Al on the part quality is noticeable. **Figure 2a** presents the SEM micrograph of the pure Cu at an ED of 185 J/mm^3. The top surface of the sample exhibits pores and bumps. Dai and Gu [15] associated this type of defects to the balling phenomenon, that leads to an increase in the surface roughness. The modeling of the behavior of the molten pool has showed the generation of driving forces such as the thermo-capillary force and the recoil pressure caused by evaporation [16]. With the heat loss, the amount of liquid metal decreases, leading to an unstable molten pool. Furthermore, applying an insufficient ED on Cu leads to a poorly melted powder, thus, to a weak wetting due to the surface tension, resulting in the formation of pores and bumps. Hence, microscale liquid droplets splash from the molten pool to form spheres [17,18].

SEM micrographs of the Cu-Al 3D printed parts with the same ED are presented in **Figures 2b - d**. The microstructures are less porous than the pure Cu. As can be seen, with 0.75 and 1.5 wt.% Al, the surfaces are smooth and the laser tracks can be identified. With 3 wt.% Al, pores were formed on the sample surfaces. Hence, adding a small amount of Al is beneficial to reinforcing the wetting behavior and the connection among the Cu particles and hence improve their densification.

On the other hand, some studies have reported the influence of the ED on the porosity formation and defect creation during the printing process [19]. A low ED was found to be insufficient to fully melt the powder. Medium and high EDs reduces the porosity. Nevertheless, keyholes and other defects can be observed in case of overheating. **Figure 2e** shows high density values for 1.5 wt.% Al at all EDs. For 0.75 and 3 wt.% Al, the densities are lower than that with 1.5 wt.% Al. As for pure Cu, the low-density values confirm the presence of voids inside the samples. Furthermore, the surface roughness of the Cu-Al parts decreased by two times compared with that of the pure Cu starting from 200 J/mm^3 as shown in **Figure 2f.** Nevertheless, the difference is not significant among the different Cu-Al parts.

The results have also shown a decrease in the density for the 3 wt.% Al. This can be explained by the oxidation of Al during the LPBF process **(Figure 2S)**. Although the oxygen content inside the printing chamber is low, it is not sufficiently low to avoid a spontaneous reaction with Al.

Consequently, if Al oxide (alumina) is formed, the laser-matter interaction is reduced. The laser power applied is insufficient to melt alumina. Furthermore, alumina cannot be wetted by molten Al (contact angle > 65º from 680 to 1100 ºC) [20]. Consequently, voids are created within the samples, causing the failure of the printing [21]. This reaction is likely to occur and has a significant impact on the printing process when the Al content exceeds a specific value.

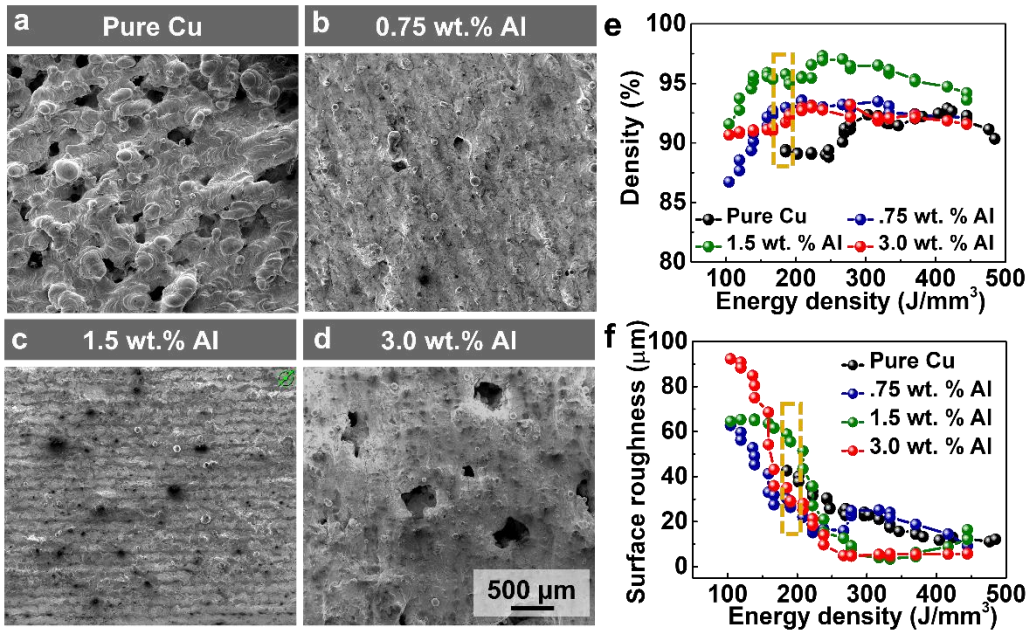

Figure 2. SEM micrographs of **a** pure Cu, and Cu with **b** 0.75, **c** 1.5, **d** 3 wt.% Al, **e** Density and **f** Surface roughness of the parts *vs.* ED.

To better understand the powder behavior during the printing process **(Figure 3d)**, we examined the melting mechanism of the powder more closely by applying the laser for a short time on a single-layered Cu-Al powder bed with 1.5 wt.% Al (**Figure 3b)**. The melting/solidification of the particles in the reaction zone is illustrated in **Figure 3a**. The powder located at the vicinity of the molten pool was extracted and analyzed using SEM. The micrographs in **Figures 3c-e** show particles that are bonded and partially fused to form a larger cluster. An EDS mapping analysis was performed on the particles observed to identify their chemical compositions. **Figure 3g** shows a strong green color corresponding to Al, particularly at the edges of two Cu powder particles schematized by the red color **(Figure 3f)**. In fact, the Al powder surrounding the molten pool was also heated and melted because of its low melting point (660 ºC) as compared with Cu

(1084 ºC) [22]. Therefore, Al is rapidly fused around the Cu powders, which clearly promotes the preliminary densification.

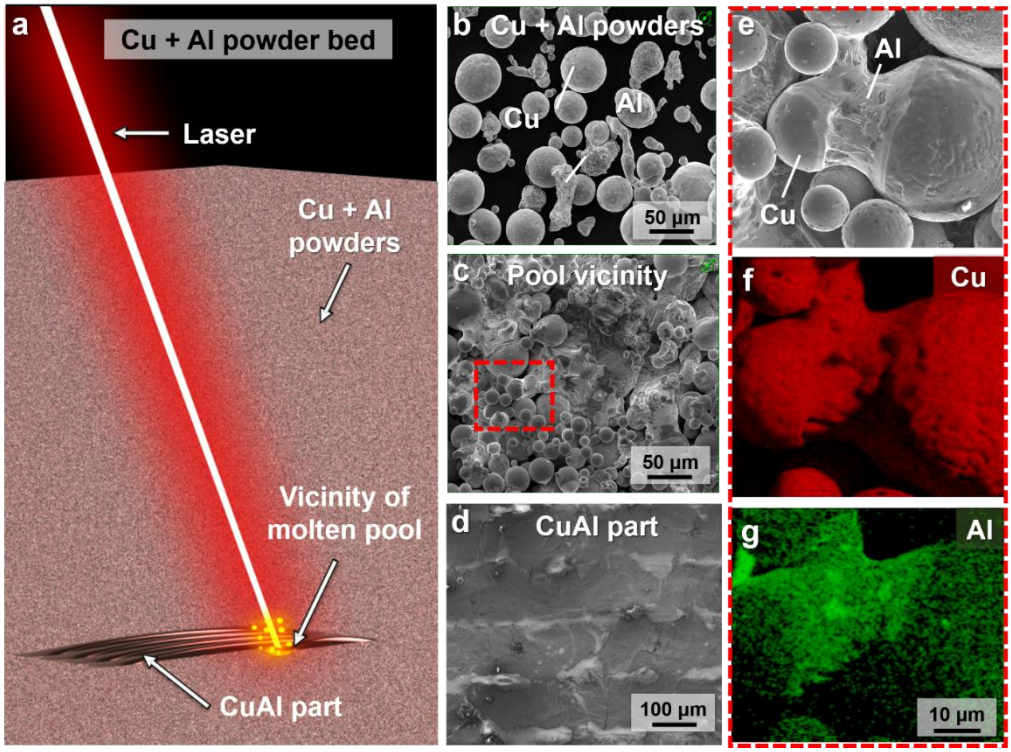

Figure 3. a Schematic representation of the LPBF of Cu-Al powders, **b** SEM micrograph of Cu-Al powders, **c** SEM micrograph of the pool vicinity, **d** SEM micrograph of the printed surface of a Cu-Al part, and **e, f, g** SEM-EDX micrographs of the pool vicinity.

The Al particles contribute to reduce pores and voids, leading to a greater surface finish. Also, the laser energy required to 3D print dense parts was significantly reduced. As a result, the temperature within the molten pool, and the resultant thermal gradient was decreased. Unlike printing Cu, the printing process of Cu-Al materials seemed to be less violent and more stable.

Figure 4a provides a summary of the pre-densification mechanism induced by Al particles during the LPBF. At a time of t_1, the laser is applied on the powder bed to instantly create a molten pool, where both Cu and Al are heated and melted. At t_2, the heat is transferred through the surrounding powder to the surrounding zones, where a thermal gradient is created (heat diffuses from the heated to cooler areas). In 3D printing, a part of the heat generated can be dissipated from the molten zone to the vicinity, to form an intense metal vapor.

The generated heat in the vicinity is less important than in the molten zone. Therefore, the heat impact on the surrounding powder is less. Nevertheless, according to the previous EDX map analysis, Al is more likely to melt when the laser-generated heat reaches the vicinity areas. At t_3, Al particles fused and then solidified, creating bonds among Cu particles. XRD was performed on the samples printed for crystalline and phase evaluation, as shown in **Figure 4b.** The diffraction peaks at $2\theta = 43\ ^{o}$, $50\ ^{o}$ and $75\ ^{o}$ correspond to (111), (200) and (220) planes, respectively, of the face-cubic-centered Cu [23]. Hence, this confirms that the 3D printed Cu-Al parts form a solid solution. Apart from Cu peaks, no other peaks were detected. The lattice constant for each composition was calculated via the Le-Bail method using the FullProf Suite. The experimentally obtained values were compared to the calculated ones. The results are plotted in **Figure 4c.** For pure Cu and Cu with 0.75 wt.% Al, both values are close. However, the measured values measured for Cu with 1.5 and 3 wt.% Al deviates from the calculated ones. In fact, the lattice parameter and the Al content are linear up to a maximum Al concentration, upon which the calculated lattice parameter deviates from Vegard`s law at a constant temperature [24].

A high-resolution TEM was performed on pure Cu and Cu with 1.5 wt.% Al samples. The micrographs in **Figures 4d-e** show the arrangement of the atoms within the prepared slices. The interplanar distance was found to be similar for both samples. It can be noticed that adding Al

has also contributed to the formation of crystallographic defects such as dislocations and reduction in the stacking fault energy [25].

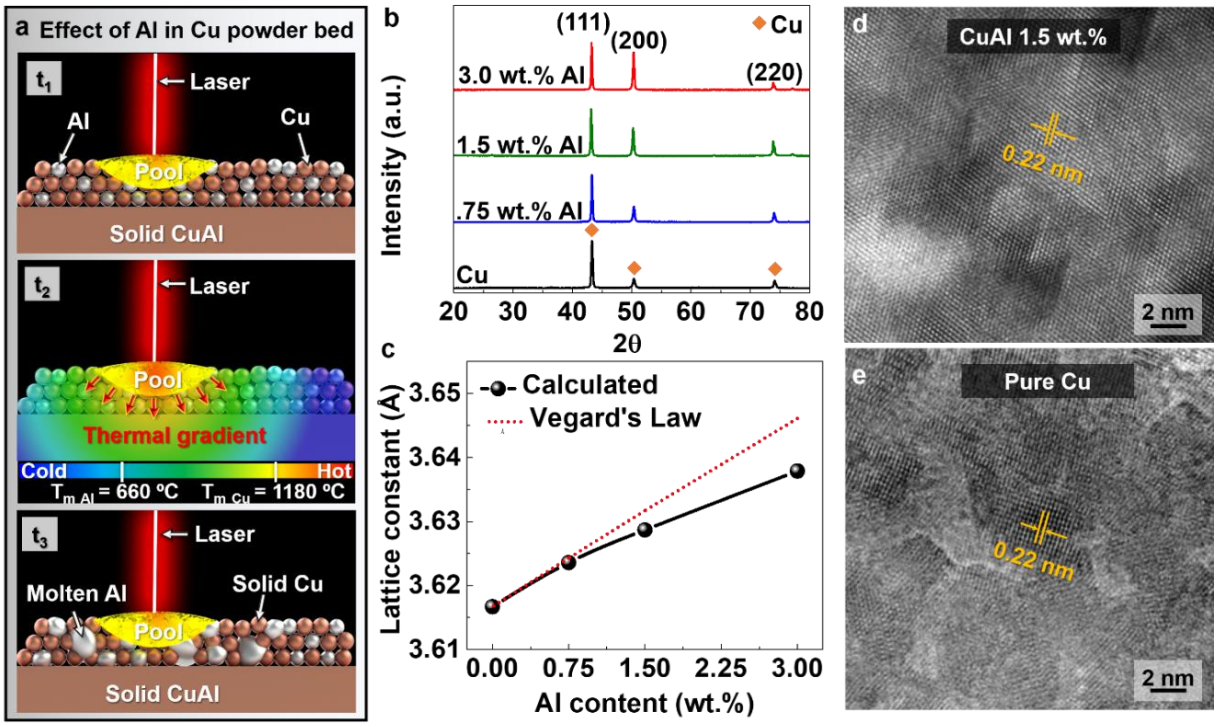

Figure 4. **a** Illustration of the effect of Al in Cu powder during the 3D printing process, **b** XRD patterns of the 3D printed samples, **c** Lattice constant as a function of the Al content, **d** HR-TEM of 1.5 wt.% Al in Cu, and **e** HR-TEM of pure Cu.

Next, the LPBF of triply periodic minimal surface (TPMS) heat exchangers was performed using the pure Cu powders and Cu-Al mixtures, where gyroid structures were successfully printed using the optimized parameters for each composition. This unusual geometric configuration offers the possibility to print lightweight heat sinks with a large specific surface area, that is beneficial to the heat dissipation performance [26,27,28]. As can be seen on **Figure 5a**, the as-

obtained complex shapes have thin and smooth features forming a large specific surface area. Note that a clear color variation was detected on the structures when increasing the Al content. The heat dissipation performance was measured for Cu with 3 wt.% Al, and then compared to pure Cu. **Figure 5b** shows the experiment set up , where the heat sinks were attached on a memory card chip using a thermal tape (3M™ 8815 Thermal Tape). The whole system was placed on a hot plate heated to 200 ºC. An IR camera (FLIR E85 24°) was used to mimic a microelectronics thermal management situation to measure the temperature of the chip. The entire system was heated to 200 ºC. An airflow was provided by a fan placed 10 cm away from the parts. Note that this experimental set-up was first established by Constantin *et al.* [7] for the thermal dissipation evaluation of pure Cu. **Figures 5b** and **c** show the plot of the chip temperature with respect to the Al content, and IR images of the gyroid structures at 200 ºC. As can be seen, when the chip is placed alone on the heated plate, the measured temperature was around 169 ºC. After attaching the pure Cu heat sink to the chip, the chip temperature was reduced by 36 ºC (T_{chip} = 133 ºC). With a gyroid composition of 0.75 wt.% Al, the dissipated heat has led to a chip temperature of T_{chip} = 138 ºC (-31 ºC). Increasing the Al content to 1.5 wt.% and 3 wt.% Al of the gyroid structures has also contributed to the thermal dissipation process, leading to a chip temperature of T_{chip} = 141 ºC (-28 ºC) and 146 ºC (-23 ºC), respectively. Clearly, the addition of Al has maintained the chip temperature lower than 169 ºC. Also, it can be noticed that increasing Al from 0 to 3 wt.% has slightly reduced the heat dissipation performances of the Cu-Al structures. In fact, several researchers have demonstrated that, adding increased amounts of an alloying element to pure Cu contributes to gradually decreased the TC of the material due to a lower ability to conduct the heat [29]. In the current

research, the SLM of Cu-Al has not only allowed to produce dense and smooth parts but also it has enabled the 3D printing of intricate shapes with great heat dissipation performance.

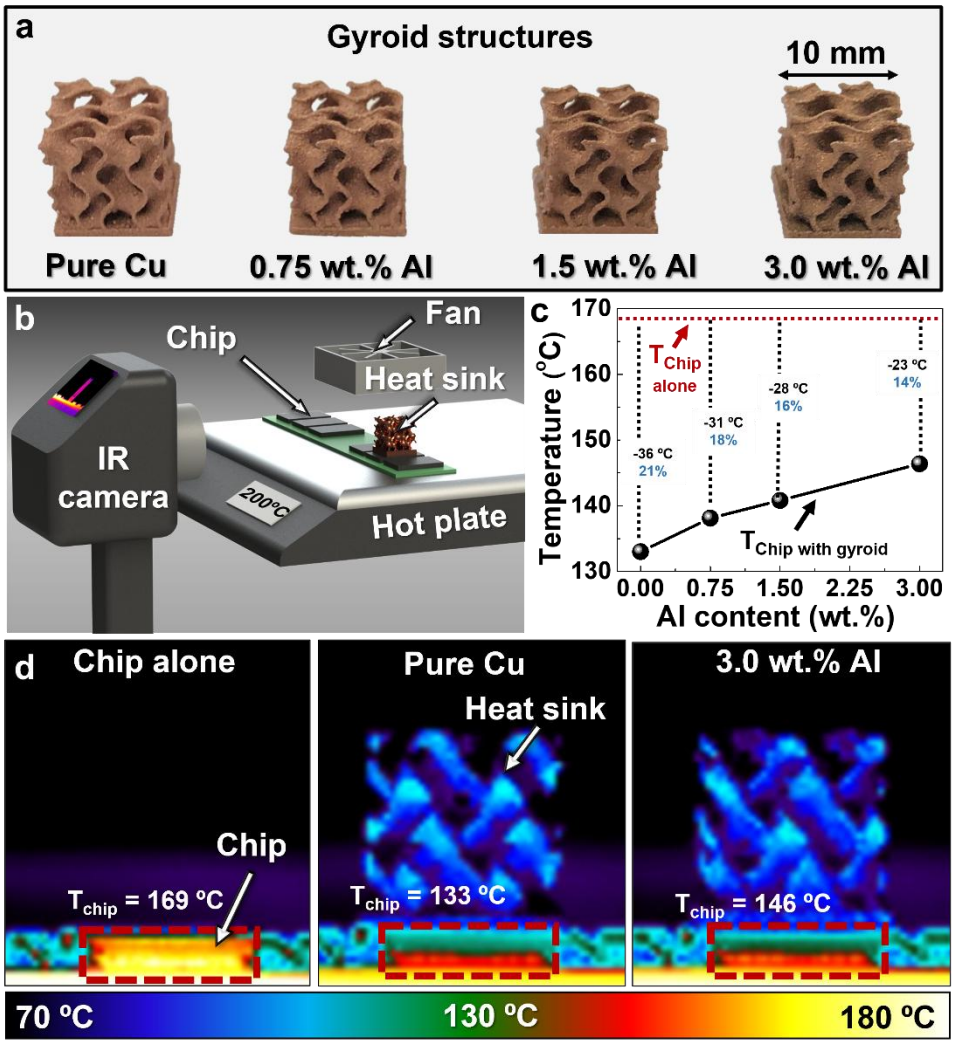

Figure 5.a Gyroid structures printed, **b** Illustration of the thermal dissipation measurement, **c** Chip temperature as a function of the Al content, and **d** IR images of chip alone and with heat sinks of pure Cu and Cu with 3 wt.% Al.

Conclusion

In this study, the influence of adding Al powder in Cu powder on 3D printing was investigated. Dense and smooth Cu alloys can be printed with a large process window (i.e., scan speed and hatch distance). The results show that adding small quantities of a lightweight metal, such as Al, improves the printability of Cu, where high ED are no longer required for the SLM process. Furthermore, the as-printed Cu-Al parts were denser than the case of pure Cu, exhibiting highly smooth, flat, and pore-free surfaces. Complex Cu-Al gyroid structures with high heat performance were also achieved using the optimized parameters. The reported results show that a composition of Cu with 1.5 wt.% Al would be the best content to obtain Cu-Al parts with high printing quality.

A further improvement of the processability of reflective metals (*e.g.*, Cu, Al, silver) and eventually ceramics would be a great benefit to additive manufacturing applications that will lead to highly advanced multi-functional materials.

Data availability

Data generated during or analyzed during the current study are included in this published article and its Supplementary Information file.

AUTHOR INFORMATION

Corresponding Authors

*Jean-François Silvain : jean-francois.silvain@icmcb.cnrs.fr; Yong Feng Lu :ylu2@unl.edu.

Author Contributions

‡ Mrs. Nada Kraiem and Dr. Loic Constantin contributed equally to this work. All authors approved the final version.

Acknowledgment

This study was supported by the National Science Foundation (CMMI 1826392) and the Nebraska Center for Energy Sciences Research (NCESR). The research was performed in part in the Nebraska Nanoscale Facility: National Nanotechnology Coordinated Infrastructure and the Nebraska Center for Materials and Nanoscience, which are supported by the National Science Foundation under Award ECCS: 1542182, and the Nebraska Research Initiative. The authors would like to thank Jamie Eske for her help on the English editing.

References

[1] S. Pal, I. Drstvensek, Physical Behaviors of Materials in Selective Laser Melting Process, in: B. Katalinic (Ed.), DAAAM International Scientific Book, 1st ed., DAAAM International Vienna, 2018: pp. 239–256. https://doi.org/10.2507/daaam.scibook.2018.21.

[2] K.G. Prashanth, Selective Laser Melting: Materials and Applications, Journal of Manufacturing and Materials Processing. 4 (2020) 13. https://doi.org/10.3390/jmmp4010013.

[3] J.-P. Kruth, M. Badrossamay, E. Yasa, J. Deckers, L. Thijs, J. Humbeeck, Part and material properties in selective laser melting of metals, 16th International Symposium on Electromachining, ISEM 2010. (2010).

[4] X. Lingqin, C. Guang, Z. Luyu, L. Pan, Explore the feasibility of fabricating pure copper parts with low-laser energy by selective laser melting, Mater. Res. Express. 7 (2020) 106509. https://doi.org/10.1088/2053-1591/abbd08.

[5] T. Tran, A. Chinnappan, J. Lee, H.L. Nguyen, L. Tran, G. Wang, V. Vijay kumar, W.A.D.M. Jayathilaka, D. Ji, M. Doddamani, S. Ramakrishna, 3D Printing of Highly Pure Copper, Metals. 9 (2019) 756. https://doi.org/10.3390/met9070756.

[6] S. Jadhav, S. Dadbakhsh, L. Goossens, J.-P. Kruth, J. Humbeeck, K. Vanmeensel, Influence of selective laser melting process parameters on texture evolution in pure copper, Journal of Materials Processing Technology. 270 (2019) 47–58. https://doi.org/10.1016/j.jmatprotec.2019.02.022.

[7] L. Constantin, Z. Wu, N. Li, L. Fan, J.-F. Silvain, Y.F. Lu, Laser 3D printing of complex copper structures, Additive Manufacturing. 35 (2020) 101268. https://doi.org/10.1016/j.addma.2020.101268.

[8] S. Zhang, H. Zhu, L. Zhang, W. Zhang, H. Yang, X. Zeng, Microstructure and properties of high strength and high conductivity Cu-Cr alloy components fabricated by high power selective laser melting, Materials Letters. 237 (2018). https://doi.org/10.1016/j.matlet.2018.11.118.

[9] J. Kruth, P. Mercelis, J. Van Vaerenbergh, L. Froyen, M. Rombouts, Binding mechanisms in selective laser sintering and selective laser melting, Rapid Prototyping Journal. 11 (2005) 26–36. https://doi.org/10.1108/13552540510573365.

[10] L. Lü, J.Y.H. Fuh, Y.S. Wong, Selective Laser Sintering, in: L. Lü, J.Y.H. Fuh, Y.S. Wong (Eds.), Laser-Induced Materials and Processes for Rapid Prototyping, Springer US, Boston, MA, 2001: pp. 89–142. https://doi.org/10.1007/978-1-4615-1469-5_5.

[11] M. Naeem, Laser Processing of Reflective Materials, Laser Technik Journal. 10 (2013) 18–20. https://doi.org/10.1002/latj.201390001.

[12] M. Yakout, M. Elbestawi, S.C. Veldhuis, S. Nangle-Smith, Influence of thermal properties on residual stresses in SLM of aerospace alloys, Rapid Prototyping Journal. 26 (2020) 213–222. https://doi.org/10.1108/RPJ-03-2019-0065.

[13] A. Majeed, Y. Zhang, J. Lv, T. Peng, Z. Atta, A. Ahmed, Investigation of T4 and T6 heat treatment influences on relative density and porosity of AlSi10Mg alloy components manufactured by SLM, Computers & Industrial Engineering. 139 (2020) 106194. https://doi.org/10.1016/j.cie.2019.106194.

[14] S. Pal, G. Lojen, N. Gubeljak, V. Kokol, I. Drstvensek, Melting, fusion and solidification behaviors of Ti-6Al-4V alloy in selective laser melting at different scanning speeds, Rapid Prototyping Journal. 26 (2020) 1209–1215. https://doi.org/10.1108/RPJ-07-2019-0206.

[15] D. Dai, D. Gu, Tailoring surface quality through mass and momentum transfer modeling using a volume of fluid method in selective laser melting of TiC/AlSi10Mg powder, International Journal of Machine Tools and Manufacture. 88 (2015) 95–107. https://doi.org/10.1016/j.ijmachtools.2014.09.010.

[16] A. Razavykia, E. Brusa, C. Delprete, R. Yavari, An Overview of Additive Manufacturing Technologies—A Review to Technical Synthesis in Numerical Study of Selective Laser Melting, Materials. 13 (2020) 3895. https://doi.org/10.3390/ma13173895.

[17] Y. Bai, C. Zhao, D. Wang, H. Wang, Evolution mechanism of surface morphology and internal hole defect of 18Ni300 maraging steel fabricated by selective laser melting, Journal of Materials Processing Technology. 299 (2022) 117328. https://doi.org/10.1016/j.jmatprotec.2021.117328.

[18] L. Chen, Y. Sun, L. Li, X. Ren, Microstructure evolution, mechanical properties, and strengthening mechanism of TiC reinforced Inconel 625 nanocomposites fabricated by selective laser melting, Materials Science and Engineering: A. 792 (2020) 139655. https://doi.org/10.1016/j.msea.2020.139655.

[19] Č. Donik, J. Kraner, I. Paulin, M. Godec, Influence of the Energy Density for Selective Laser Melting on the Microstructure and Mechanical Properties of Stainless Steel, Metals. 10 (2020) 919. https://doi.org/10.3390/met10070919.

[20] S. Bao, K. Tang, A. Kvithyld, M. Tangstad, A. Engh, Wettability of Aluminum on Alumina, Metallurgical and Materials Transactions B. 42 (2011) 1358–1366. https://doi.org/10.1007/s11663-011-9544-z.

[21] E. Louvis, P. Fox, C.J. Sutcliffe, Selective laser melting of aluminium components, Journal of Materials Processing Technology. 211 (2011) 275–284. https://doi.org/10.1016/j.jmatprotec.2010.09.019.

[22] N. Ponweiser, C.L. Lengauer, K.W. Richter, Re-investigation of phase equilibria in the system Al–Cu and structural analysis of the high-temperature phase η1-Al1−δCu, Intermetallics. 19 (2011) 1737–1746. https://doi.org/10.1016/j.intermet.2011.07.007.

[23] Q. Zhang, Z. Qin, Q. Luo, Z. Wu, L. Lei, B. Shen, W. Hu, Microstructure and nanoindentation behavior of Cu composites reinforced with graphene nanoplatelets by electroless co-deposition technique, Scientific Reports. 7 (2017). https://doi.org/10.1038/s41598-017-01439-3.

[24] J. Zhang, R.E. Hackenberg, E.B. Watkins, S.C. Vogel, D.W. Brown, The lattice parameter – composition relationship of the body centered cubic uranium-niobium alloys, Journal of Nuclear Materials. 542 (2020) 152493. https://doi.org/10.1016/j.jnucmat.2020.152493.

[25] R. Goswami, P. Pao, S. Qadri, R. Holtz, Severe Plastic Deformation Induced Sensitization of Cryo-milled Nanocrystalline Al-7.5 Mg, Metallurgical and Materials Transactions A. 45 (2014). https://doi.org/10.1007/s11661-014-2227-z.

[26] O. Alketan, D.-W. Lee, R. Rowshan, R. Abu Al-Rub, Functionally graded and multi-morphology sheet TPMS lattices: Design, manufacturing, and mechanical properties, Journal of the Mechanical Behavior of Biomedical Materials. 102 (2019) 103520. https://doi.org/10.1016/j.jmbbm.2019.103520.

[27] E. Gawrońska, R. Dyja, A Numerical Study of Geometry's Impact on the Thermal and Mechanical Properties of Periodic Surface Structures, Materials. 14 (2021) 427. https://doi.org/10.3390/ma14020427.

[28] I. Kaur, P. Singh, Flow and thermal transport characteristics of Triply-Periodic Minimal Surface (TPMS)-based gyroid and Schwarz-P cellular materials, Numerical Heat Transfer, Part A: Applications. 79 (2021) 553–569. https://doi.org/10.1080/10407782.2021.1872260.

[29] G. Abbas Gohar, T. Manzoor, A.N. Shah, Investigation of thermal and mechanical properties of Cu-Al alloys with silver addition prepared by powder metallurgy, Journal of Alloys and Compounds. 735 (2018) 802–812. https://doi.org/10.1016/j.jallcom.2017.11.176.